Astron. Astrophys. 241, 625–634 (1991)

ASTRONOMY AND ASTROPHYSICS

Propagation of nonlinear longitudinal-transverse waves along magnetic flux tubes in the solar atmosphere

I. Adiabatic waves

P. Ulmschneider[1], K. Zähringer[1], and Z. E. Musielak[2]

[1] Institut für Theoretische Astrophysik, Universität Heidelberg, Im Neuenheimer Feld 561, D–6900 Heidelberg, Federal Republic of Germany

[2] Center for Space Plasma and Aeronomic Research, University of Alabama, Huntsville, AL 35899, USA

Received July 10; accepted August 8, 1990

Abstract. The nonlinear time-dependent response to purely transverse foot point shaking of a vertical magnetic flux tube in the solar atmosphere was studied. The adiabatic calculations show the generation of a longitudinal wave mode which has twice the frequency of the transverse wave. The amplitude of the longitudinal wave increases with the wave period and with the magnitude of the shaking. Due to the action of centrifugal forces significant lifting of the tube gas was found. A forced oscillator type resonance occurs which depends on the tube length.

Key words: magnetic flux tubes, waves, chromosphere

1. Introduction

We consider the propagation of nonlinear adiabatic magnetohydrodynamic waves in intense thin magnetic flux tubes embedded in the otherwise field-free solar atmosphere. Since the discovery of the highly inhomogeneous magnetic flux distribution at the solar surface (Stenflo 1978, Zwaan 1978, see also Stenflo et al. 1987) the propagation of magnetohydrodynamic (mhd) wave propagation in magnetic flux tubes has been extensively studied (starting with e.g. Defouw, 1976; Roberts and Webb, 1978, 1979; Wilson, 1979; Parker, 1979; Wentzel 1979). For more recent discussions see e.g. Edwin and Roberts (1983), Herbold et al. (1985) as well as Molotovshchikov and Ruderman (1987).

Spruit (1982) as well as Edwin and Roberts (1983) have shown that in the thin, intense fluxtube geometry there are several wave modes possible: a *torsional mode*, the nonlinear propagation of which has been studied by Hollweg et al. (1982), and recently by Anton (1989), a *transverse mode* and a *longitudinal mode*. The nonlinear behaviour of the longitudinal wave mode has been investigated by Herbold et al. (1985) who found that these waves behave essentially like acoustic tube waves. These authors found that a main difference between acoustic and longitudinal tube waves is the propagation speed. The former propagates with the sound speed c_S and the latter with the tube speed c_T.

Send offprint requests to: P. Ulmschneider

The attention given to the study of mhd waves is only partly explained by the fact that they are an interesting phenomenon of the outer solar atmosphere. A main reason for the great interest in these waves lies in the fact, that mhd waves may be one of the basic mechanisms both for the generation of *hot chromospheric and coronal layers* around late-type stars (see e.g. Stein and Leibacher 1980, Kuperus et al. 1985, Ulmschneider 1986, Narain and Ulmschneider 1990) and for the production of *stellar winds* (see e.g. Hartmann and McGregor 1980, Dupree 1986, Cuntz 1987, An et al. 1990). For the very tight correlation of the magnetic flux density and the chromospheric emission flux see Schrijver et al. (1989). It is highly likely that mhd waves constitute one of the prime energy carriers from the stellar envelope to the regions where the UV and X-ray radiation and the stellar wind flows originate. Thus all aspects of the waves, their generation, propagation and dissipation are of great importance.

For the *dissipation* of mhd waves see the review articles of Kuperus et al. (1985) or Narain and Ulmschneider (1990). As the acoustic-like longitudinal mhd waves easily form shocks they clearly represent an efficient dissipation mechanism. Yet it seems more difficult to directly dissipate transverse and torsional waves. The *generation* of mhd waves is little understood. A simple dimensional analysis by Stein (1981) and Ulmschneider and Stein (1982) predicts considerable wave energy flux for both longitudinal and transverse waves. However, recent computations of the production of longitudinal waves in solar convection zone tubes by linear buffeting from the turbulent convection give little energy (Musielak et al. 1987, 1989). As there are errors in these calculations (see Musielak et al. 1990) and as there are large scale distorsions of the flux tubes by the granular flows the energy production of these waves is probably considerably larger. In the transition layer, where the flux tubes are thought to occupy the entire available space, Athay and White (1978) observe little acoustic energy. This is consistent with the picture that the longitudinal waves are dissipated by shocks, which makes the longitudinal waves a prime candidate for the heating of the low and middle chromosphere.

An alternative method for the production of longitudinal waves is the *nonlinear mode-coupling* from other wave types as discussed by Wentzel (1974, see also Narain and Ulmschneider 1990). Mode-coupling permits the scenario that transverse or

torsional waves carry the energy into the outer layers where the dissipation is eventually affected by longitudinal shock waves. This could be the way by which the high chromosphere is heated. Musielak et al. (1990) find considerable transverse mhd wave energy production. Nonlinear mode-coupling as a viable process which converts torsional to longitudinal waves has been found by Hollweg et al. (1982) and by Anton (1989).

In the present work we aim to explore the nonlinear behaviour of transverse tube waves in detail and in particular study the mode-coupling between transverse and longitudinal waves. For preliminary results of the present study see Zähringer and Ulmschneider (1987), Ulmschneider and Zähringer (1987) as well as Ulmschneider and Musielak (1990). These results indicate that mode-coupling indeed is very important for transverse waves. In Section 2, following Spruit (1981) we derive the mhd tube wave equations valid for thin tubes. Section 3 shows how these equations are solved using the characteristics method. The initial magnetic tube model and the applied boundary conditions are described in Section 4. Section 5 discusses the results of our coupled transverse-longitudinal wave computations using different wave excitations and boundary conditions. Conclusions are given in Section 6.

2. Basic equations

2.1. Magnetohydrodynamic equations

The behaviour of longitudinal-transverse mhd tube waves is governed by the basic time-dependent mhd equations (Landau and Lifshitz 1960, p. 218), by the continuity equation, the equation of motion, the induction equation in the limit of large electrical conductivity, and the energy equation in the form of the entropy conservation equation:

$$\frac{\partial \rho}{\partial t} + \nabla \cdot \rho \mathbf{v} = 0 , \tag{1}$$

$$\rho \left(\frac{\partial \mathbf{v}}{\partial t} + \mathbf{v} \cdot \nabla \mathbf{v} \right) = -\nabla p - \frac{1}{4\pi} \mathbf{B} \times (\nabla \times \mathbf{B}) + \rho \mathbf{g} , \tag{2}$$

$$\frac{\partial \mathbf{B}}{\partial t} = \nabla \times (\mathbf{v} \times \mathbf{B}) , \quad \text{with} \quad \nabla \cdot \mathbf{B} = 0 , \tag{3}$$

$$\frac{\partial S}{\partial t} + \mathbf{v} \cdot \nabla S = \left. \frac{\mathrm{dS}}{\mathrm{dt}} \right|_{\mathrm{Rad}} . \tag{4}$$

Here ρ is the density, $\mathbf{v}$ the velocity, p the gas pressure, $\mathbf{B}$ the magnetic field strength, $\mathbf{g}$ the gravitational acceleration, S the entropy and t the time. For the radiative heating function $dS/dt|_{Rad}$ various forms may be used (see Herbold et al. 1985, Ulmschneider and Muchmore 1986). In the present paper we assume adiabatic waves and take $dS/dt|_{Rad} = 0$. In a nonionizing gas we have the ideal gas equation

$$p = \rho \frac{\Re}{\mu} T , \tag{5}$$

and the thermodynamic relation

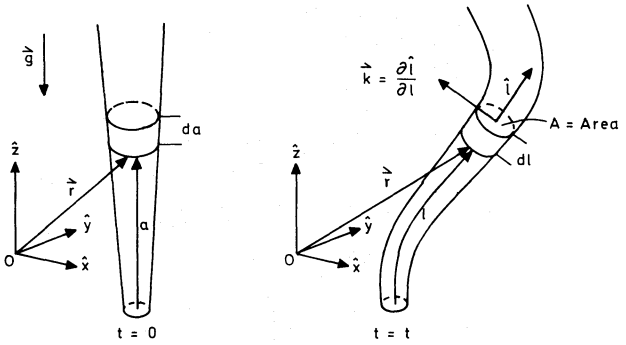

Fig. 1. Flux tube geometry

$$\frac{\rho}{\rho_R} = \left(\frac{c_S}{c_{S_R}} \right)^{\frac{2}{\gamma - 1}} e^{-\mu (S - S_R)/\Re} , \tag{6}$$

where $\Re = 8.31 \cdot 10^7$ *erg/mol K* is the gas constant, $\mu = 1.3$ *g/mol* the mean molecular weight and $\gamma = 5/3$ the ratio of specific heats. Subscript R denotes a fixed reference state. The sound speed c_S is given by

$$c_S^2 = \gamma \frac{p}{\rho} . \tag{7}$$

2.2. Flux tube geometry

We assume a vertically oriented magnetic flux tube of circular cross-section A (c.f. Fig. 1) embedded in an otherwise non-magnetic atmosphere. The position of the fluid particles in the tube can be either described by the radius vector $\mathbf{r}$ in a laboratory (Euler) frame $(\hat{\mathbf{x}}, \hat{\mathbf{y}}, \hat{\mathbf{z}})$, where the z-axis is in vertical direction, or in a locally cylindrical coordinate system $(\hat{\mathbf{s}}, \hat{\mathbf{e}}_\phi, \hat{\mathbf{l}})$ by the arc-length l measured from the bottom of the tube and where the unit arc-length vector $\hat{\mathbf{l}}$ points along the local tube axis. We restrict ourselves to purely one-dimensional wave propagation and consider a thin flux tube (Spruit 1981), where the tube spreading, that is, the ratio of the components $B_s/B_l = ds/dl$, is much smaller than one.

In our one-dimensional description we replace the physical quantities of the fluid particle in the tube by mean values, averaged over the cross-section. Moreover we assume that the tube radius is always much smaller than the radius of curvature r_k of the tube. This is necessary to ensure that the fluid particles can be descibed by a unique and reversible relation between $\mathbf{r}$ and l. The magnetic field is assumed to point in $\hat{\mathbf{l}}$ direction:

$$\mathbf{B} = \mathrm{B} \hat{\mathbf{l}} , \tag{8}$$

with the magnetic flux given by

$$\Phi = B A = const . \tag{9}$$

To restrict ourselves to purely longitudinal-transverse waves we further assume that there is no ϕ-component or ϕ-dependence.

With the multidimensional non-magnetic atmosphere outside the tube the description of the gas motion in a thin flux tube is

still a multidimensional problem. To reduce the spatial order of the problem further, we assume that the external atmosphere is static (i.e. does not depend on time) and varies only with height z. The error made by this assumption can only be assessed if more detailed multidimensional computations are made. Unfortunately these computations are presently not available. In addition, in the thin flux tube approximation one has horizontal pressure balance

$$p + \frac{B^2}{8\pi} = p_e(z) , \tag{10}$$

where the external gas pressure $p_e(z)$ is independent of time. This incompressible assumption for the outside medium is certainly a poor one, particularly as the considered horizontal velocities are not small against the sound speed. Yet this assumption greatly simplifies our problem and allows us to study the pure mode coupling process without energy loss into the outside medium.

Let a be the height measured from the bottom of the tube to the fluid particle in the initially undisturbed vertically oriented tube at time $t = 0$ (Fig. 1). This height a is called *Lagrange height* and uniquely identifies the considered fluid particle. We want to describe all physical variables as functions of the independent variables a and t. At some later time, due to the tube displacement and the gas motion in the tube, the fluid particle originally at Lagrange height a will be displaced to a position given by the arc-length $l(a, t)$. The equation of continuity requires that

$$\rho(a,t)\, A(a,t)\, dl\,|_t = \rho_o(a)\, A_o(a)\, da , \tag{11}$$

where A is the cross-section of the tube and subscript 0 denotes values in the undisturbed atmosphere at time $t = 0$. We define a scale factor

$$l_a \equiv \left(\frac{\partial l}{\partial a}\right)_t = \frac{\rho_o A_o}{\rho A} . \tag{12}$$

From Eqs. (11) or (12) we have

$$l(a,t) = \int_o^a \frac{\rho_o A_o}{\rho A}\, da \Bigg|_t . \tag{13}$$

With the radius vector $\mathbf{r}$ given by $\big(x(a,t), y(a,t), z(a,t)\big)$ we have for the unit vector $\hat{\mathbf{l}}$

$$\hat{\mathbf{l}} = (l_x, l_y, l_z) = \left(\frac{\partial \mathbf{r}}{\partial \mathrm{l}}\right)_t = \frac{1}{l_a}\left(\frac{\partial \mathbf{r}}{\partial \mathrm{a}}\right)_t , \tag{14}$$

with

$$l_x^2 + l_y^2 + l_z^2 = 1 . \tag{15}$$

From the differential

$$\begin{aligned} df &= \left[\left(\frac{\partial \mathbf{r}}{\partial \mathrm{a}}\right)_t \cdot \nabla\right] f\, da + \left[\left(\frac{\partial \mathbf{r}}{\partial \mathrm{t}}\right)_a \cdot \nabla + \frac{\partial}{\partial t}\right] f\, dt \\ &= \left(\frac{\partial f}{\partial a}\right)_t da + \left(\frac{\partial f}{\partial t}\right)_a dt \end{aligned} , \tag{16}$$

using Eq. (14) and identifying terms, we obtain the transformation equations between the Euler and the Lagrange frames

$$\left(\frac{\partial f}{\partial a}\right)_t = l_a \hat{\mathbf{l}} \cdot \nabla f , \quad \left(\frac{\partial f}{\partial t}\right)_a = \left(\frac{\partial}{\partial t} + \mathbf{v} \cdot \nabla\right) \mathrm{f} , \tag{17}$$

where the velocity is given by

$$\mathbf{v} = \left(\frac{\partial \mathbf{r}}{\partial \mathrm{t}}\right)_a . \tag{18}$$

The curvature vector $\mathbf{k}$ and the radius of curvature r_k are defined (see Fig. 1) by

$$\mathbf{k} \equiv \left(\frac{\partial \hat{\mathbf{l}}}{\partial \mathrm{l}}\right)_t = \frac{1}{l_a}\left(\frac{\partial \hat{\mathbf{l}}}{\partial \mathrm{a}}\right)_t \perp \hat{\mathbf{l}} , \quad \mathrm{r_k} \equiv \frac{1}{|\mathbf{k}|} . \tag{19}$$

We now want to write Eqs. (1) to (4) in the Lagrange frame and decompose these equations into longitudinal and transverse components. For any vector $\mathbf{A}$ one has

$$\mathbf{A}_{\parallel} = (\hat{\mathbf{l}} \cdot \mathbf{A})\, \hat{\mathbf{l}} , \quad \mathbf{A}_{\perp} = (\hat{\mathbf{l}} \times \mathbf{A}) \times \hat{\mathbf{l}} . \tag{20}$$

The transverse component of Eq. (2) reads

$$\begin{aligned} \rho\left[\left(\frac{\partial \mathbf{v}}{\partial \mathrm{t}}\right)_a - \left[\hat{\mathbf{l}} \cdot \left(\frac{\partial \mathbf{v}}{\partial \mathrm{t}}\right)_a\right] \hat{\mathbf{l}}\right] &= -\left[\hat{\mathbf{l}} \times \nabla\left(p + \frac{B^2}{8\pi}\right)\right] \times \hat{\mathbf{l}} \\ &\quad + \frac{B^2}{4\pi}\mathbf{k} + \rho\,(\hat{\mathbf{l}} \times \mathbf{g}) \times \hat{\mathbf{l}} \end{aligned} , \tag{21}$$

where Eqs. (3), (8), (17), (19) and the relation

$$\mathbf{B} \times (\nabla \times \mathbf{B}) = \frac{1}{2}\nabla \mathrm{B}^2 - \mathrm{B}\hat{\mathbf{l}}\, \frac{\partial \mathrm{B}}{\partial \mathrm{l}} - \mathrm{B}^2\, \frac{\partial \hat{\mathbf{l}}}{\partial \mathrm{l}} , \tag{22}$$

have been used. We assume that the external medium is in hydrostatic equilibrium

$$\nabla p_e = \rho_e \mathbf{g} , \tag{23}$$

and modify the pressure gradient term using Eq. (10). The transverse motion of the tube will displace the external gas. To crudely take into account the apparent increase of inertia of the fluid particle in the tube due to this sweeping action on the external gas we follow Basset (1961) and Spruit (1981) and replace the density ρ in the inertial term on the LHS of Eq. (21) by $\rho + \rho_e$. Note that this procedure critically depends on our circular choice of the cross-section, as the amount of displaced external material will depend on the shape which the tube presents in the direction of the swaying. We find

$$\begin{aligned} \left(\frac{\partial \mathbf{v}}{\partial \mathrm{t}}\right)_a - \left[\hat{\mathbf{l}} \cdot \left(\frac{\partial \mathbf{v}}{\partial \mathrm{t}}\right)_a\right] \hat{\mathbf{l}} &= \frac{\rho c_A^2}{\rho + \rho_e}\, \frac{1}{l_a}\left(\frac{\partial \hat{\mathbf{l}}}{\partial a}\right)_t \\ &\quad + \frac{\rho - \rho_e}{\rho + \rho_e}\left(\mathbf{g} + \mathrm{g}\mathrm{l}_z \hat{\mathbf{l}}\right) \end{aligned} . \tag{24}$$

Here we have introduced the Alfvén speed c_A,

$$c_A^2 = \frac{B^2}{4\pi\rho} . \tag{25}$$

For the longitudinal component of Eq. (2) we have with Eq. (17)

$$\rho\hat{\mathbf{l}}\cdot\left(\frac{\partial \mathbf{v}}{\partial t}\right)_a = -\frac{1}{l_a}\left(\frac{\partial p}{\partial a}\right)_t - \rho g l_z , \tag{26}$$

where the Lorentz forces, which are perpendicular to $\hat{\mathbf{l}}$, do not contribute. With Eqs. (5) to (7) we eliminate the pressure in favour of c_S and S and obtain

$$\hat{\mathbf{l}}\cdot\left(\frac{\partial \mathbf{v}}{\partial t}\right)_a + \frac{1}{l_a}\left[\frac{2c_S}{\gamma-1}\left(\frac{\partial c_S}{\partial a}\right)_t - \frac{c_S^2\mu}{\gamma\Re}\left(\frac{\partial S}{\partial a}\right)_t\right] + g l_z = 0 . \tag{27}$$

Expanding the RHS of the induction equation (3), using Eqs. (1) and (17) we have

$$\left(\frac{\partial \mathbf{B}}{\partial t}\right)_a = (\mathbf{B}\cdot\nabla)\mathbf{v} - \mathbf{B}\nabla\cdot\mathbf{v} = (\mathbf{B}\cdot\nabla)\mathbf{v} + \frac{\mathbf{B}}{\rho}\left(\frac{\partial \rho}{\partial t}\right)_a . \tag{28}$$

With Eq. (8) the transverse component of this equation is

$$\left(\frac{\partial \hat{\mathbf{l}}}{\partial t}\right)_a = \frac{1}{l_a}\left[\left(\frac{\partial \mathbf{v}}{\partial a}\right)_t - \hat{\mathbf{l}}\cdot\left(\frac{\partial \mathbf{v}}{\partial a}\right)_t\hat{\mathbf{l}}\right] , \tag{29}$$

where B has been cancelled. The longitudinal component of Eq. (28) reads

$$\left(\frac{\partial B}{\partial t}\right)_a = \frac{B}{\rho}\left(\frac{\partial \rho}{\partial t}\right)_a + \frac{B}{l_a}\hat{\mathbf{l}}\cdot\left(\frac{\partial \mathbf{v}}{\partial a}\right)_t . \tag{30}$$

The time derivative of Eq. (10) gives

$$\frac{\rho c_A^2}{B}\left(\frac{\partial B}{\partial t}\right)_a = \left(\frac{\partial}{\partial t}(p_e - p)\right)_a = v_z\frac{dp_e}{dz} - \left(\frac{\partial p}{\partial t}\right)_a , \tag{31}$$

which is used to eliminate the magnetic field term in Eq. (30). Replacing the derivatives of p and ρ in favour of those of c_S and S we finally have for the longitudinal component of Eq. (28)

$$\frac{\hat{\mathbf{l}}}{l_a}\cdot\left(\frac{\partial \mathbf{v}}{\partial a}\right)_t + \frac{2c_S}{\gamma-1}\frac{1}{c_T^2}\left(\frac{\partial c_S}{\partial t}\right)_a - \frac{\mu}{\gamma\Re}\left(\frac{c_S^2}{c_A^2}+\gamma\right)\left(\frac{\partial S}{\partial t}\right)_a - \frac{v_z}{\rho c_A^2}\frac{dp_e}{dz} = 0 . \tag{32}$$

Here we have introduced the tube speed

$$c_T = \left(\frac{c_S^2 c_A^2}{c_S^2 + c_A^2}\right)^{\frac{1}{2}} . \tag{33}$$

In summary, for the 8 unknowns c_S, S , $\mathbf{v}$, $\hat{\mathbf{l}}$ of the one-dimensional longitudinal-transverse mhd tube wave problem, we have seven partial differential equations and Eq. (15). There are one longitudinal- (Eq. 27) and two transverse (Eq. 24) components of the equation of motion, one longitudinal- (Eq. 32) and two transverse (Eq. 29) components of the combined induction and continuity equations, and from Eqs. (4) and (17) the entropy conservation equation

$$\left(\frac{\partial S}{\partial t}\right)_a = \left.\frac{dS}{dt}\right|_{Rad} , \tag{34}$$

where for our present adiabatic application $dS/dt|_{Rad} = 0$.

3. Method of characteristics

In order to numerically solve the system of time-dependent longitudinal-transverse tube wave equations we follow our work on acoustic- and longitudinal waves (Ulmschneider et al., 1977, Herbold et al., 1985), and select the method of characteristics. This method has been found to be very efficient for problems where the characteristic time scale is the Courant time (Hammer and Ulmschneider 1978). By a proper linear combination of the partial differential equations from the above set we derive ordinary differential equations along specific characteristic directions. These characteristic directions are themselves given by ordinary differential equations and represent the world lines in the a, t plane along which infinitesimally small disturbances travel.

From a linear combination of Eqs. (27), (32) and (34), that is, the longitudinal components of the equation of motion and the induction/continuity equations and the energy equation, we find after some algebra

$$\hat{\mathbf{l}}\cdot d\mathbf{v} \pm \frac{2}{\gamma-1}\frac{c_S}{c_T}dc_S \mp \frac{\mu c_S^2}{\gamma\Re c_T}dS \mp \left[\frac{\mu c_T}{\gamma\Re}(\gamma-1)\left.\frac{dS}{dt}\right|_{Rad} + \frac{v_z c_T}{\rho c_A^2}\frac{dp_e}{dz} \mp g l_z\right]dt = 0 , \tag{35}$$

along the two characteristics C_1^+, C_1^- given by

$$\left(\frac{da}{dt}\right)_\pm = \pm\frac{c_T}{l_a} . \tag{36}$$

Here the top sign in Eqs. (35) and (36) is for the C_1^+ and the bottom sign for the C_1^- characteristic. Note that for purely vertical propagation, where $l_z = 1$, Eqs. (35) and (36) reduce to the longitudinal tube wave equations of Herbold et al. (1985, their Eqs. 53, 54). Combining Eqs. (24) and (29), i.e. the transverse components of the equation of motion and the induction/continuity equations, we find after some algebra the two equations

$$\begin{aligned}\left(1-l_x^2\right)dv_x - l_x l_y dv_y - l_x l_z dv_z \mp c_k dl_x - \frac{\rho-\rho_e}{\rho+\rho_e}g l_x l_z dt &= 0 ,\\ \left(1-l_y^2\right)dv_y - l_x l_y dv_x - l_y l_z dv_z \mp c_k dl_y - \frac{\rho-\rho_e}{\rho+\rho_e}g l_y l_z dt &= 0 ,\end{aligned} \tag{37}$$

both along the two characteristics C_2^+, C_2^- given by

$$\left(\frac{da}{dt}\right)_\pm = \pm\frac{c_k}{l_a} . \tag{38}$$

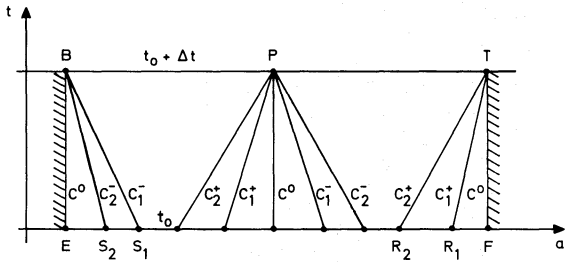

Fig. 2. Space-time diagram of the computational domain showing the various characteristics

where c_k is the propagation speed of the pure transverse wave given by

$$c_k = c_A \sqrt{\frac{\rho}{\rho + \rho_e}} . \tag{39}$$

The top sign in Eqs. (37) and (38) is for the C_2^+ and the bottom sign for the C_2^- characteristic. Note that the pure longitudinal wave propagates with the tube speed c_T. For a discussion of the two characteristic tube speeds c_k and c_T see e.g. Edwin and Roberts (1983). Finally Eq. (34) is integrated along the C^0- or fluid path characteristic $a = const$:

$$dS = \left(\frac{\partial S}{\partial t}\right)_a dt = \left.\frac{dS}{dt}\right|_{Rad} dt . \tag{40}$$

Fig. 2 shows the characteristics network between two consecutive time steps in the a, t plane for an interior point P and for the two boundary points B, T. The characteristics for the three considered points are indicated. The physical state in the tube is supposed to be known on the a axis between the boundary points E and F at time t_o. At the interior point P the 8 unknown variables at the time $t_o + \Delta t$ are uniquely determined by solving in addition to Eq. (15) the 7 ordinary differential equations, (35), (37) and (40) along the 5 characteristics. As the method of characteristics explicitly follows the physics of the information flow, it is well suited for the discussion of the nature of the boundary conditions which have to be applied in our longitudinal-transverse wave computation. Fig. 2 shows, that for the bottom and top boundary points, B and T, respectively, due to missing characteristics, *exactly* three boundary conditions each must be given.

4. Boundary and initial conditions

4.1. Boundary conditions

Both at the top and the bottom of the tube, sets of boundary conditions have to be chosen. At the *top boundary*, where we want the waves to exit without reflection we have adopted transmitting boundary conditions. Here we follow our acoustic calculations (Ulmschneider et al. 1977) and assume that, similarly as for large amplitude simple waves, the velocity amplitude remains constant along the outgoing C_1^+ and C_2^+ characteristics. To facilitate the specification of boundary velocities we introduce three perpendicular unit vectors $\hat{\mathbf{l}}_1, \hat{\mathbf{l}}_2, \hat{\mathbf{l}}_3$. We assume that $\hat{\mathbf{l}}_3 \equiv \hat{\mathbf{l}}$ is identical to the arc-length vector $\hat{\mathbf{l}}$, that $\hat{\mathbf{l}}_1$ lies in the x, z plane, and that $\hat{\mathbf{l}}_2$ is perpendicular to $\hat{\mathbf{l}}_1$ and $\hat{\mathbf{l}}_3$ in such a way, that $\hat{\mathbf{l}}_1, \hat{\mathbf{l}}_2, \hat{\mathbf{l}}_3$ form a right hand system. With the components of $\hat{\mathbf{l}}$ given, the two vectors $\hat{\mathbf{l}}_1$ and $\hat{\mathbf{l}}_2$ can be computed using

$$\hat{\mathbf{l}}_1 = \frac{\hat{\mathbf{y}} \times \hat{\mathbf{l}}}{|\hat{\mathbf{y}} \times \hat{\mathbf{l}}|} = \frac{1}{\sqrt{l_x^2 + l_z^2}} \begin{bmatrix} l_z \\ 0 \\ -l_x \end{bmatrix} , \tag{41}$$

$$\hat{\mathbf{l}}_2 = \hat{\mathbf{l}} \times \hat{\mathbf{l}}_1 = \frac{1}{\sqrt{l_x^2 + l_z^2}} \begin{bmatrix} -l_x l_y \\ l_x^2 + l_z^2 \\ -l_y l_z \end{bmatrix} . \tag{42}$$

If the indices 1, 2, 3 indicate components along $\hat{\mathbf{l}}_1, \hat{\mathbf{l}}_2, \hat{\mathbf{l}}_3$, the conditions at the *top boundary* point T can be written

$$v_{1T} = v_{1R2} \ , \ v_{2T} = v_{2R2} \ , \ v_{3T} = v_{3R1} . \tag{43}$$

Here R_1, R_2 refer to the foot points of the C_1^+, C_2^+ characteristics (c.f. Fig. 2). For the *bottom boundary* conditions we choose two cases. For both cases in this study of transverse waves, we horizontally shake the bottom of the tube and consider only linearly polarized waves in x- direction. The two cases concern the treatment of the longitudinal wave. The *closed case* assumes a tube with a closed bottom as in an organ pipe. For this case we assume at the bottom boundary point B:

$$\text{Closed :} \quad v_{1B} = -v_0 \sin(2\pi \frac{t}{P}) \ , \ v_{2B} = 0 \ , \ v_{3B} = 0 , \tag{44}$$

where v_0 is the specified velocity amplitude of the shaking and P the shaking period. The *open case* assumes an open tube where the longitudinal wave is allowed to exit downwards:

$$\text{Open :} \quad v_{1B} = -v_0 \sin(2\pi \frac{t}{P}) \ , \ v_{2B} = 0 \ , \ v_{3B} = v_{3S1} . \tag{45}$$

Here S_1 is the foot point of the C_1^- characteristic (c.f. Fig. 2). Note that in both the open and closed cases the waves are excited by *purely* transverse oscillations.

4.2. Initial flux tube model

For the time-dependent wave calculation one needs an initial atmosphere and flux-tube model. These models were computed similar as by Herbold et al. (1985). For the external atmosphere we took a grey radiative and hydrostatic equilibrium model, computed with the two beam approximation. As the tube is assumed thin, the radiation field in the tube is determined by the external field which leads to temperature equality between the tube and its surroundings at every given height. With the specification of a tube radius of 50 *km* and a magnetic field strength of 1500 *G* at the height where in the external atmosphere the optical depth $\tau_{5000} = 1$, the physical state of the tube is uniquely determined. This tube we call *exponential tube*. The height of the exponential tube is limited to less than 1200 km because above this range the criterion $B_s/B_l < 1$ for thin flux tubes breaks down.

However, due to neighbouring tubes exponential spreading becomes unrealistic at these heights anyway. To crudely take into account neighbouring tubes we have modified the exponential tube above the height 500 km to allow only linear spreading. This is achieved by artificially raising the external gas pressure in accordance with Eq. (10). The external density is likewise changed to satisfy hydrostatic equilibrium. The increased external pressure is supposed to roughly simulate the external magnetic pressure

Table 1. Diameter d_0 in *km*, magnetic field strength B_0 in *G*, external and internal gas pressure p_e and p_0 in dyn/cm^2, temperature T in *K*, sound speed c_S, Alfvén speed c_A, tube speed c_T, transverse wave speed c_K in *km/s* as function of height a in *km* for our linear tube model.

a	d_0	B_0	p_e	p_0	T	c_S	c_A	c_T	c_K
0	100	1500	1.38E5	4.82E4	6001	8.0	10.9	6.6	5.6
340	208	344	7.25E3	2.53E3	4688	7.1	10.6	5.9	5.4
670	386	101	5.28E2	1.26E2	4681	7.1	13.8	6.3	7.0
1000	561	48	9.63E1	5.87E0	4681	7.1	30.4	6.9	16.

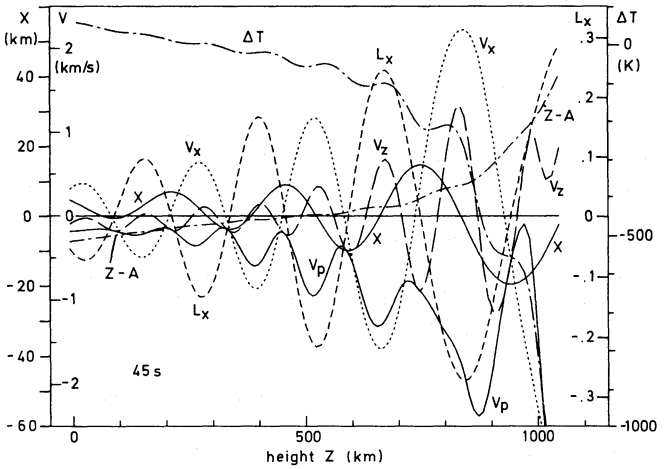

Fig. 3. Snapshot of a longitudinal- transverse wave of period $P = 45$ *s* at time 600 *s* after pure transverse sinusoidal shaking at the bottom has started with a velocity amplitude of $v_0 = 0.4$ *km/s*. Horizontal v_x, vertical v_z and parallel v_p velocity components, horizontal Δx and vertical $z - a$ displacements as well as the temperature T are shown as function of height z. Note that v_z and v_p are multiplied by a factor of 5 to facilitate the presentation.

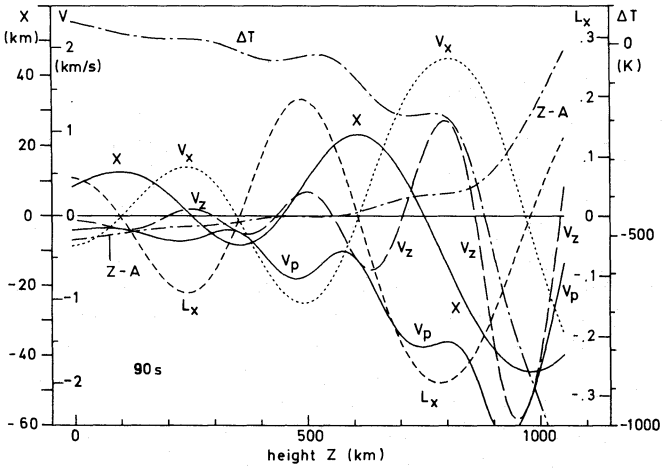

Fig. 4. Same as Fig. 3, however with period $P = 90$ *s*.

excerted from neighbouring tubes; likewise the increased external density should simulate the increased inertia. The resulting *linear tube* is assumed to represent the conditions of the chromospheric network and spreads with height as shown in Tab. 1.

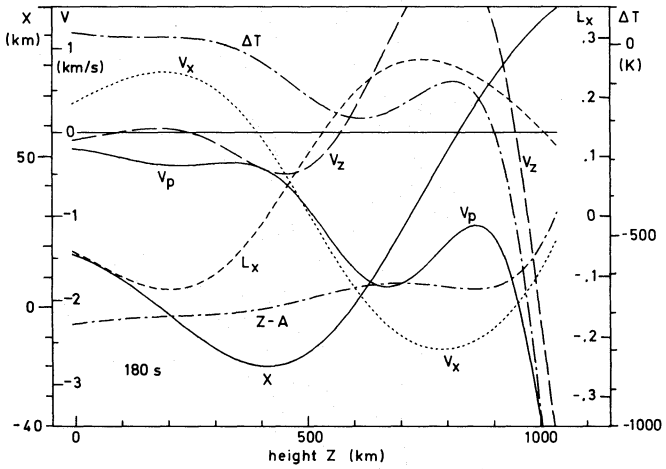

Fig. 5. Same as Fig. 3, however with period $P = 180$ *s*.

5. Results

For the linear open tube case we have solved the time-dependent equations described above for adiabatic waves of periods $P =$ 45, 90, 180, 300 *s* and purely transverse shaking at the bottom with velocity amplitudes $v_0 = 0.2$, 0.4, 0.8, 1.6 *km/s*. From these computations Figs. 3 to 6 show snapshots at the time $t = 600$ *s* of waves with periods $P = 45$, 90, 180, 300 *s*, all with the same shaking velocity amplitude $v_0 = 0.4$ *km/s*.

5.1. Height dependence of the wave properties

The *horizontal velocity* v_x is seen to grow rapidly with height. This is a consequence of wave energy flux conservation. As the transverse wave speed c_k is roughly constant over a large fraction of the tube (c.f. Tab. 1), flux conservation, $\rho v_x^2 c_k \approx const$, implies that the amplitude of the velocity v_x behaves roughly like $\rho^{-1/2}$ and thus grows similarly in all four Figs. Strict flux conservation would imply an amplitude of $v_x = 1.5$ *km/s* at 340 km height, while only $v_x = 0.8$ *km/s* is found in Figs. 3 or 4. This shows that the transverse wave flux is only approximately conserved. The reasons for this are discussed below.

The *horizontal displacement* Δx is seen to trail v_x by $\pi/2$ in phase, with maxima at the nodes of v_x and nodes at the maxima of v_x. The velocity component v_x and the *direction cosine* l_x have a phase difference of π. For the wave propagating in vertical direction these facts are explained as follows. If at a node of Δx the inclination of the tube in the $\pm$x-direction is largest, then the fluid particle because of the frozen-in condition suffers the

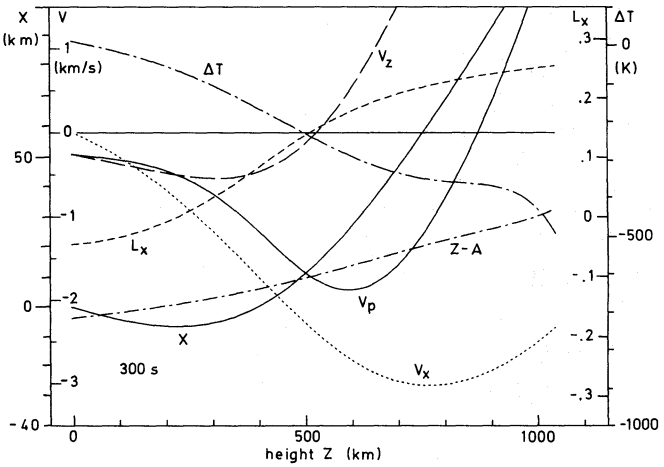

Fig. 6. Same as Fig. 3, however with period $P = 300$ *s*.

largest rate of displacement in $\mp$x- direction, being pushed out of the way by the advancing B-field. v_x and l_x have the same spatial frequency k_0. x oscillates around a value $x_0 = v_0 P/(2\pi)$ obtained by integrating Eq. (45). The profile x versus height gives the actual geometrically distorted shape of the tube axis.

An interesting property is that the maximum swaying amplitude Δx increases with the wave period. For the waves of Figs. 3 to 6 the maximum horizontal swaying amplitudes Δx are 20, 45, 100, 130 *km* at periods $P = 45$, 90, 180, 300 *s* respectively. Although there is a considerable increase of the swaying amplitude by a factor of 6, it is seen from Tab. 1 that these displacements are still only a fraction of the tube diameter. The reason for the increased swaying amplitude with wave period is the similar dependence of the velocity amplitudes v_x on height for the waves of Figs. 3 to 6 of identical excitation amplitude v_0. The longer integration timespan for longer wave periods then leads to greater excursions $\Delta x = \int v_x dt$.

5.2. *Appearance of a longitudinal wave*

In addition to the horizontal velocities, *vertical velocity components* v_z appear. Figs. 3 to 6 show that v_z (and l_z) has a spatial frequency of $2k_0$, twice as large as that of the components v_x and l_x. This is understood from the fact that the direction cosine l_z goes through two cycles for every one cycle of l_x, because after Eq. (15) the sign of l_x does not affect the magnitude of l_z. The reason for the appearance of these longitudinal (compressional) velocity components is the action of the curvature forces which are always perpendicular to the local tube direction, c.f. Eq. (19). These forces have horizontal and vertical components. In one wavelength of the Δx profile the vertical force component changes sign twice while the horizontal force component only once. It is the action of the vertical force component which leads to rarefactions and compressions of the gas and thus to a longitudinal wave.

As already noted above, there is only approximate flux conservation for the transverse wave. Part of the wave energy is used to feed the longitudinal wave mode. This is seen from the fact that the amplitude of v_z increases spectacularly by about a factor of 16, 30, 70, 140 over the entire height range for the waves with period $P = 45$, 90, 180, 300 *s*, respectively. Yet the longitudinal wave flux is only a fraction of the transverse wave flux. As we will discuss below, the missing transverse wave energy flux is spent mainly on the work done in lifting the tube gas.

Strictly speaking the vertical velocity component v_z is not the longitudinal velocity. The component parallel to the tube is defined by

$$v_p = l_x v_x + l_y v_y + l_z v_z. \tag{46}$$

Figs. 3 to 6 show the parallel velocity component v_p and its rapid increase with height. It is seen that v_p, similar to v_z, has a spatial frequency of $2k_0$ but contrary to that component is entirely negative. This behaviour of v_p is explained as follows: The product $l_x v_x$, due to the phase difference of π, as shown in Figs. 3 to 6, is always negative and because v_x is much larger than v_z leads to a negative main contribution in Eq. (46). The same product is also responsible for the doubling of the spatial frequency. That v_p is persistently negative, appears to contradict the mean upward mass flow necessary for the lifting (see Sec. 5.3). This apparent contradiction is due to a projection effect: v_p results from a total velocity vector, directed predominantly horizontally but slightly vertically (generating the lifting), projected onto a considerably inclined tube axis.

The nonlinear coupling of the longitudinal and transverse wave types generates a whole spectrum of different spatial frequencies. Fig. 3 shows that v_p in addition to the dominant spatial frequency $2k_0$ also has the fundamental frequency k_0 as seen by the fact that every second amplitude is characteristically different in size. In addition the term $v_z l_z$ in Eq. (46) produces a series of higher orders of k_0.

Because long period waves have more extensive swaying excursions Δx, they suffer greater gas pressure fluctuations. This results in a greater longitudinal wave energy generation for long period waves: In Figs. 3 to 6 the ratio of the velocity maxima v_z/v_x near 800 *km* height is 1/9, 1/8, 1/6, 1/4 for the waves with $P = 45$, 90, 180, 300 *s*, respectively.

5.3. *Lifting due to centrifugal forces*

As already mentioned above, an interesting effect found in our calculations is the lifting of the gas column in the tube. We attribute this effect to *centrifugal forces* introduced by the increase of the swaying with height. Swayings in $\pm$x- directions both result in outwardly directed force components. Figs. 3 to 6 show the lifting $z - a$ of the fluid element originally at height a as function of height. The topmost points in Figs. 3 to 6 after the swaying has operated for 600 *s*, are lifted upwards by 30 to 40 *km*, roughly independent of the wave period. This lifting continues at later times as shown in Fig. 8.

As is seen from the temperature distributions $\Delta T = T(z) - T_0(a)$ in Figs. 3 to 6, this lifting leads to adiabatic cooling which is more extensive towards the top of the tube. As the gas is lifted to greater height the gas pressure there is increased, and due to horizontal pressure balance, the tube expands, whereby the magnetic field strength decreases. The oscillations in the temperature distributions with twice the fundamental frequency, $2k_0$, indicate that they are associated with the longitudinal wave. This is also seen by the small phase difference between ΔT and v_z in Figs. 3 and 4.

The bottom of the tube moved down into the sun by about 7 *km*. This effect depends on the chosen boundary condition and on the magnitude of the swaying as seen in Fig. 7. In calculations

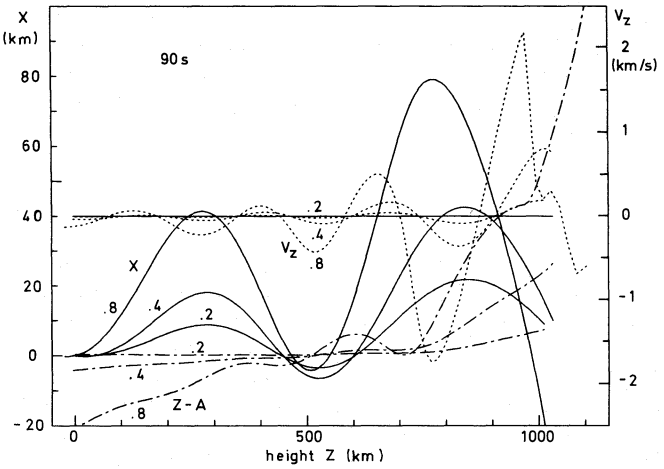

Fig. 7. Longitudinal-transverse waves of period P= 90 s at time t=450 s, excited by different velocity amplitudes $v_0 = 0.2, 0.4, 0.8$ *km /s*. The vertical velocity v_z, the height shift $z - a$ and the horizontal displacement Δx are shown.

with a *closed case* boundary the tube bottom showed an opposite behaviour and was lifted by a comparable amount. In these closed tube cases the entire tube atmosphere was lifted which has already been found by Zähringer and Ulmschneider (1987).

5.4. Other tube models

So far the computations involved a linear open or closed tube model. We now want to discuss a few other model computations. For a similar excitation as for the linear tube model we found for an *exponential tube model* (see Sec. 4.2) that although the results were rather similar at low height they differed considerably at great height. This behaviour is expected as below the height 500 *km* both tube models are identical. At great height the swaying amplitude in the exponential tube became much larger than for the linear tube as the outside gas pressure in the exponential tube is much smaller. Due to the increased swaying, the lifting, the adiabatic cooling and longitudinal velocity component generation were all strongly magnified.

Another case investigated by us was a linear tube model with the magnitude of the magnetic field reduced from 1500 *G* to 1000 *G*. Aside of the fact that the different Alfvén speed lead to a much smaller wavelength for a given excitation period, the amount of lifting, adiabatic cooling and longitudinal velocity component generation was not much different from the corresponding strong field case. Both the exponential tube and the 1000 *G* tube cases were computed only for curiosity and are not very realistic. The exponential case because the magnetic fields are not permitted to spread unperturbed by neighbouring fields, and the 1000 *G* field case because it violates the requirement that at photospheric heights the tubes are nearly empty and the magnetic field strength obeys $B^2/8\pi \approx p_e$. We hencefourth stay with the linear open tube model of Tab. 1.

5.5. Dependence on the intensity of swaying

As nonlinear mode-coupling effects increase with the amplitude we expect that the ratio v_z/v_x increases with increasing excitation amplitude v_0. For the $P = 90$ *s* wave of Fig. 4, two additional snapshots at similar times but with different excitation amplitudes are shown in Fig. 7, which demonstrate that this expectation is indeed true. The ratio v_z/v_x near 670 *km* height is found to be 1/15, 1/8.2, 1/6.8 if $v_0 = 0.2$, 0.4, 0.8 *km/s*, respectively. Near the top of the tube these ratios increase rapidly. Thus the ratio of longitudinal to transverse wave energy increases with increasing swaying amplitude.

The amount of lifting also depends on the swaying velocity v_0. It is seen that the top point is lifted by 7, 30, 110 *km* for for the swaying amplitudes of $v_0 = 0.2$, 0.4, 0.8 *km/s*, respectively. It should be noted that with swaying amplitudes of $v_0 = 0.8 km/s$ and larger, the horizontal velocities v_x became supersonic after a short propagation time of the wave. Here the validity of our equations becomes questionable. In addition, to be consistent with our one- dimensional description, it is necessary to ensure that the radius of curvature of the tube stays larger than the tube radius. This condition limits the excitation amplitude. In our cases with $P = 45s$ we find, that the waves should have initial velocity amplitudes $v_0 < 0.5$ *km/s*. This is valid for the linear tube, for the exponential tube the excitation amplitude must be much smaller.

5.6. Resonance effects

The time-development of the swaying of purely transversely excited flux tubes is shown in Figs. 8a and 8b. Both cases have the same excitation amplitude $v_0 = 0.2$ *km/s* and wave period $P = 300s$. Horizontal velocity amplitudes of this magnitude of the solar five minute oscillations have been observed by Title (1987) in the SOUP experiment. Transverse wave calculations using these excitation parameters have been discussed by Ulmschneider and Zähringer (1987). Different from their work based on exponential tubes we assume here linear open tube models.

Fig. 8a shows 25 consecutive phases of the horizontal deviation Δx of the tube axis versus height separated by 75 $s = 1/4$ wave period. The starting model was purely vertical with $\Delta x = 0$ at time $t = 0$ *s*. It is seen that in phases 1 and 2, at $t = 75$ and 150 *s*, the wave did not have time enough to completely cross the model. The length ≈ 1000 *km* of our tube model was chosen to be about 1/4 of the wavelength λ. Fig. 8a shows that in response to the shaking with constant amplitude, the swaying amplitude at greater height first increases rapidly with time and then, after about 5 wave periods, reaches a maximum. We attribute this to a resonance situation similarly as in a forced oscillator. Such a resonance depends strongly on the tube length, as is shown below.

The deviation of the flux tube by about 9° from the vertical direction leads to magnetic field oscillations with amplitudes of about 16 percent for the B_x and 1.3 percent for the B_z component. Our calculations show that the magnetic field strength B decreases secularly with time due to the mass flow towards the top, as discussed in Sec. 5.3. The lifting of the tube gas at the upper part of the flux tube can be seen in Fig. 8a (and 8b) by the height dependence of the top of the tube. Fig. 8a shows that the top of the tube after 1875 s is lifted by 100 km and that this lifting process continues vigorously.

Fig. 8b shows an identical wave calculation to that of Fig. 8a which uses the same linear open tube except that the tube length has now been decreased from 1000 km to 800 km. The same phases as in Fig. 8a are shown, plotted on similar scales. That the excitation and initial state of the tube are identical is

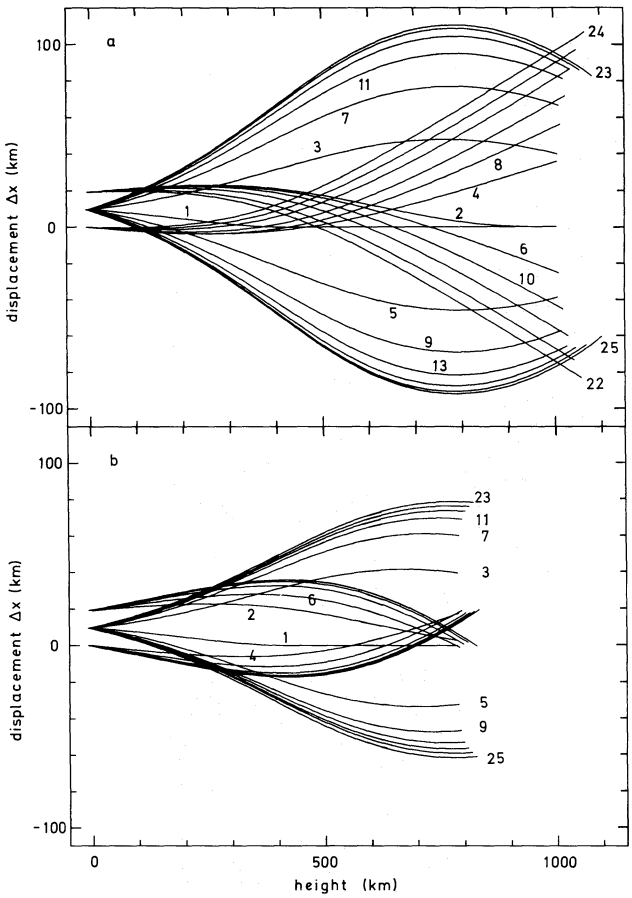

Fig. 8. Snapshots of a longitudinal- transverse wave of period $P = 300$ *s* with excitation amplitude of $v_0 = 0.2$ *km/s* shown at 25 consecutive (numbered) phases 75 *s* appart. Only the horizontal displacements Δx are shown. Panels a and b show the results for tubes of 1000 and 800 km length, respectively

seen by the fact that the phases 1 and 2 are the same in Figs. 8a and 8b. The smaller tube length in Fig. 8b decreases the height below the $\approx \lambda/4$ value. By comparing Figs. 8a and 8b it is seen that the increase of the swaying amplitude with time and the maximum swaying amplitude as well as the lifting are all much smaller in the shorter tube case. This shows that the tube height plays a critical role for the occurrence of resonances in the shaking amplitudes as is expected from the analogy with the gas oscillations in an organ pipe. For realistic situations it is not clear what the choice of a different tube height means. A realistic tube does not end at a certain height and is not independent of its neighbours. It is true that the canopy height can be widely different in active and quiet regions. The present work shows that the height over which it can be considered a single entity plays an important role. However, a realistic behaviour of the swaying can only be simulated if radiative damping effects are taken into account.

6. Conclusions

The nonlinear response to purely horizontal foot point shaking of vertical magnetic flux tubes was studied. Due to the approximate transverse wave flux conservation, the horizontal velocity component v_x was found to increase with height. The horizontal swaying excursions Δx were greater both with increasing height and with larger wave period. The nonlinear interactions led to a with height rapidly increasing vertical velocity component v_z with twice the spatial frequency of the transverse wave. The amplitude ratio v_z/v_x indicative of the efficiency of the longitudinal wave generation strongly increases with the wave period.

The increase of the swaying with height led to outward vertically directed centrifugal forces which produced a significant lifting of the tube gas. This lifting resulted in considerable adiabatic cooling near the top of the flux tube. The vertical velocity component and the amount of lifting were found to depend strongly on the magnitude of the shaking. The chosen tube length plays a role in the appearance of resonances, similar as for a gas column in an organ pipe. However, these resonances are difficult to interpret in view of the fact that realistic tubes do not have a finite extent and moreover have neighbors. Finally it must be stressed that the inclusion of radiation effects are urgently needed.

Acknowledgements. We thank the Deutsche Forschungsgemeinschaft for generous support of project Ul 57/11-2.

References

An, C.H., Suess, S.T., Moore, R.L., Musielak, Z.E.: 1989, *Astrophys. J.* **350**, 309
Anton, V.: 1989, *Ph. D. thesis*, Univ. of Göttingen, Germany
Athay, R.G., White, O.R.: 1978, *Astrophys. J.* **226**, 1135
Basset, A.B.: 1961, *A Treatise on Hydrodynamics*, Vol.1, Dover Publ., New York
Cuntz, M.: 1987, *Astron. Astrophys.* **188**, L5
Defouw, R.J.: 1976, *Astrophys. J.* **209**, 266
Dupree, A.K.: 1986, Ann. Rev. *Astron. Astrophys.* **24**, 377
Edwin, P.M., Roberts, B.: 1983, *Solar Physics* **88**, 179
Hammer, R., Ulmschneider, P.: 1978, *Astron. Astrophys.* **69**, 273
Hartmann, L., MacGregor, K.B.: 1980, *Astrophys. J.* **242**, 260
Herbold, G., Ulmschneider, P., Spruit, H.C., Rosner, R.: 1985, *Astron. Astrophys.* **145**, 157
Hollweg, J.V., Jackson, S., Galloway, D.: 1982, *Solar Physics* **75**, 35
Kuperus, M., Ionson, J.A., Spicer, D.S.: 1981, *Ann. Rev. Astron. Astrophys.* **19**, 7
Landau, L.D., Lifshitz, E.M.: 1960, *Electrodynamics of Continuous Media*, Addison-Wesley, Reading MA, USA
Molotovshchikov, A.L., Ruderman, M.S.: 1987, *Solar Physics* **109**, 247
Musielak, Z.E., Rosner, R., Ulmschneider, P.: 1987, in: *Cool Stars, Stellar Systems and the Sun*, Lecture Notes in Physics **291**, J.L. Linsky and R.E. Stencel Eds., Springer, Berlin, p. 66
Musielak, Z.E., Rosner, R., Ulmschneider, P.: 1989, *Astrophys. J.* **337**, 470
Musielak, Z.E., Rosner, R., Ulmschneider, P.: 1990, in: *Cool Stars, Stellar Systems and the Sun*, Astr. Soc. Pacific Conf. Ser. **9**, G. Wallerstein Ed., p. 79
Narain, U., Ulmschneider, P.: 1990, *Space Sci. Rev.*, in press
Parker, E.N.: 1979, *Cosmical Magnetic Fields*, Clarendon Press, Oxford
Roberts, B., Webb, A.R.: 1978, *Solar Physics* **56**, 5
Roberts, B., Webb, A.R.: 1979, *Solar Physics* **64**, 77

Schrijver, C.J., Coté, J., Zwaan, C., Saar, S.H.: 1989, *Astron. Astrophys.* **337**, 964
Spruit, H.C.: 1981, *Astron. Astrophys.* **98**, 155
Spruit, H.C.: 1982, *Solar Physics* **75**, 3
Stein, R.F.: 1981, *Astrophys. J.* **246**, 966
Stein, R.F., Leibacher, J.: 1980, in: *Stellar Turbulence*, IAU Colloq. No. 51, Lecture Notes in Physics **114**, D.F. Gray, J.L. Linsky Eds., Springer, Berlin, Germany, p. 225
Stenflo, J.O.: 1978, *Rep. Progr. Phys.* **75**, 3
Stenflo, J.O., Solanki, S.K., Harvey, J.W.: 1987, *Astron. Astrophys.* **171**, 305
Title, A. et al.: 1987 in: *Solar and Stellar Physics*, Lecture Notes in Physics **292**, E.H. Schröter, M. Schüssler Eds., Springer, Berlin, Germany, p.173
Ulmschneider, P.: 1979, *Space Sci. Rev.* **24**, 71
Ulmschneider, P.: 1986, *Adv. Space Res.* **6**, No. 8, 39
Ulmschneider, P., Muchmore, D.: 1986, in: *Small Scale Magnetic Flux Concentrations in the Solar Photosphere*, W. Deinzer, M. Knölker, H.H. Voigt Eds., Vandenhoeck and Ruprecht, Göttingen, Germany, p. 191
Ulmschneider, P., Musielak, Z.E.: 1990, in: *Cool Stars, Stellar Systems and the Sun*, Astr. Soc. Pacific Conf. Ser. **9**, G. Wallerstein Ed., p. 116
Ulmschneider, P., Kalkofen, W., Nowak T., Bohn, U.: 1977 *Astron. Astrophys.* **54**, 61
Ulmschneider, P., Stein, R.F.: 1982, *Astron. Astrophys.* **106**, 9
Ulmschneider, P., Zähringer, K.: 1987, in: *Cool Stars, Stellar Systems and the Sun*, Lecture Notes in Physics **291**, J.L. Linsky, R.E. Stencel Eds., Springer, Berlin, Germany, p. 63
Wilson, P.: 1979, *Astron. Astrophys.* **71**, 9
Wentzel, D.G.: 1974, *Solar Physics* **39**, 129
Wentzel, D.G.: 1979, *Astron. Astrophys.* **76**, 20
Zähringer, K., Ulmschneider, P.: 1987, in: *The Role of Fine- Scale Magnetic Fields on the Structure of the Solar Atmosphere*, E.H. Schröter, M. Vazquez, A.A. Wyller Eds., Cambridge Univ. Press, Cambridge, England, p. 243
Zwaan, C.: 1978, *Solar Physics* **60**, 213

This article was processed by the author using Springer-Verlag TEX AA macro package 1989.